Influence of atmospheric conditions on contrail formation: 3D simulation versus Schmidt- Appleman criterion

Weeded Ghedhaifi, Aurélien Bienner, Riad Megherbi, Emmanuel Montreuil, Etienne Terrenoire, Xavier Vancassel, Adrien Loseille

Influence of atmospheric conditions on contrail formation: 3D simulation versus Schmidt-Appleman criterion

W. Ghedhaïfi, A. Bienner, R. Megherbi, E. Montreuil, E. Terrenoire and X. Vancassel
weeded.ghedhaifi@onera.fr
Multi-Physics Department for Energetics, ONERA, University of Paris Saclay
F-91123 Palaiseau
France

A. Loseille
GAMMA3 project, INRIA
F-91120 Saclay
France

ABSTRACT

Condensation trails, usually called contrails, represent an increasing issue for aeronautics. Contrail formation and properties depends on several factors such as ambient atmospheric conditions (temperature and relative humidity), mainly, but also possibly on engine characteristics (e.g. bypass ratio, exhaust temperature), fuel type (e.g. kerosene or alternative fuels), and aircraft geometry (e.g. driving mixing in the aircraft wake). Therefore, parametric studies allow for a better understanding of contrails onset mechanisms and assessment of their properties sensitivity in the aircraft near field. This can help to find out smart mitigation solutions to reduce the environmental impact of contrail/induced cirrus by better controlling their formation. In this context, reliable prediction tools as well as technologies input are urgently needed for decision makers. Using the computational fluid dynamics code CEDRE, developed at ONERA and adapted for contrail issues, 3D simulations have been carried out to address this need. It takes into account the dynamical evolution of the jet plume, the chemical transformations of the exhaust after ejection and the microphysical processes driving contrails formation. The simulations are performed on a realistic aircraft configuration. The objective here is to confront 3D simulation approach with the Schmidt-Appleman criterion, widely used to determine contrails formation areas.

Keywords: Contrails; CFD; Schmidt-Appleman

NOMENCLATURE

CRM	Common Research Model
CFD	Computational Fluid Dynamics

Symbols

L_x	Length of the computational domain in the x-direction, in m
L_y	Length of the computational domain in the y-direction, in m
L_z	Length of the computational domain in the z-direction, in m
b	span of the wing, in m
$\overline{\rho}$	mean density of the gas mixture, in kg/m^3
$\overline{p}$	mean pressure of the gas mixture, in Pa
$\overline{p}_t$	mean total pressure of the gas mixture, in Pa
$\overline{T}$	mean static temperature of the gas mixture, in K
$\overline{T}_t$	mean total temperature of the gas mixture, in K
RH	Relative Humidity, in %
$\overline{N}_s$	Mean concentration of soot, in #/cm^3
$\tilde{u}_i$	Favre average velocity, ith component, in m/s
$\tilde{y}_k$	Favre average mass fraction of kth species, in kg/kg
D_k	Diffusion coefficient for the kth species, in m^2/s
c_p	Specific heat capacity at constant pressure for the gas mixture, in J/kg
μ	Dynamical viscosity of the gas mixture, in kg/(m.s)
$\tilde{e}$	Favre average internal energy of the gas mixture, in J/kg
$\tilde{e}_t$	Favre average total energy of the gas mixture, in J/kg
$\tilde{h}_t$	Favre average total enthalpy of the gas mixture, in J/kg
$\tilde{S}_{ij}^d$	Deviator strain-rate tensor, in 1/s
$\widetilde{u_i^{"}u_j^{"}}$	Reynolds Stress tensor, in m^2/s^2

1.0 INTRODUCTION

Contrails and the induced cirrus contribute significantly to the radiative forcing due to the associated cloudiness. In fact, the aviation overall radiative forcing reaches 0.08 W.m^{-2} and the part due to induced cirrus may represent 0.03 W.m^{-2} [1]. However the related uncertainty range for this value is rather large (0.02 - 0.05 W.m^{-2}) because of the multiple physical processes and scales involved, which challenge current modeling capabilities. Besides, environmental and tax policies are being established to take into account the impact of aviation on climate change, as a response to an increased political awareness.

Using the computational fluid dynamics code CEDRE [2], developed at ONERA and adapted for contrails issues, 3D simulations have been carried out to address this need. It takes into account the dynamical evolution of the jet plume, the chemical transformations of the exhaust after ejection and the microphysics related to contrail formation (see [3], [4] and [5]). The simulations are performed on a realistic aircraft configuration, which is crucial as the plume expansion and exhaust dispersion are driven by the evolution of the aircraft wake dynamics. First, we simulate the jet and the vortex behavior using the RANS approach for the selected aircraft geometry. Then, the gas phase evolution of reactive exhaust species in the jet is taken into consideration as well as their interaction with emitted soot particles. Soot act as condensation nuclei for water condensation as soon as they get surface-activated by sulfur species. Finally, ice crystals formation and subsequent growth are modelled.

In previous studies, we carried out a short sensitivity study on atmospheric relative humidity [3]. Furthermore, we evaluated the impact of fuel sulfur content on the early contrail formation [4]. However, more studies have to be done to improve current knowledge regarding contrails properties. The objective here is to confront 3D simulation approach with the Schmidt-Appleman criterion, widely used to determine contrails formation areas. The Schmidt-Appleman criterion revised by Schumann [6] is an analytical method based mainly on engines efficiency, exhaust temperature, water vapor emission index, ambient temperature and ambient humidity. It provides the temperature threshold of contrails formation. In this work, we compare CEDRE 3D simulations that give local properties within the plume in the aircraft near field and the Schmidt-Appleman predictions, especially for threshold conditions. Several simulations are carried out and analyzed for different atmospheric conditions (particularly temperature and relative humidity) in order to evaluate the sensitivity of contrail formation to meteorological conditions.

2.0 MODEL

2.1 Fluid flow

The CEDRE numerical code used for the present study is a compressible Navier-Stokes solver with multi-species [2]. Numerical methods are based on a cell-centered finite-volume approach for general unstructured grids. The differential equations related to the RANS 3D compressible Navier-Stokes equations in the code CEDRE read in:

$$\frac{\partial}{\partial t}(\overline{\rho}\tilde{y}_k) + \frac{\partial}{\partial x_j}(\overline{\rho}\tilde{u}_j\tilde{y}_k) = \frac{\partial}{\partial x_j}\left(\overline{\rho}D_k\frac{\partial \tilde{y}_k}{\partial x_j} - \widetilde{\overline{\rho}u_j^{"}y_k^{"}}\right) + \overline{\dot{\omega}}_k \qquad (1)$$

$$\frac{\partial}{\partial t}(\overline{\rho}\tilde{u}_i) + \frac{\partial}{\partial x_j}(\overline{\rho}\tilde{u}_j\tilde{u}_i) = -\frac{\partial \overline{p}}{\partial x_i} - \overline{\rho}g\delta_{i3} + \frac{\partial}{\partial x_j}\left(\mu\tilde{S}_{ij}^{d} - \widetilde{\overline{\rho}u_i^{"}u_j^{"}}\right) \qquad (2)$$

$$\frac{\partial}{\partial t}(\overline{\rho}\tilde{e}_t) + \frac{\partial}{\partial x_j}(\overline{\rho}\tilde{u}_j\tilde{h}_t) = \frac{\partial}{\partial x_j}\left(\overline{\rho}c_p\alpha\frac{\partial \overline{T}}{\partial x_j} + \sum_k \overline{\rho}\tilde{h}_t D_k\frac{\partial \tilde{y}_k}{\partial x_j} - \sum_k \overline{\rho}\tilde{h}_t\,\widetilde{u_j^{"}y_k^{"}} - \widetilde{\overline{\rho}u_j^{"}T^{"}} + 2\mu\tilde{S}_{ij}^{d} - \widetilde{\overline{\rho}u_i^{"}u_j^{"}}\tilde{u}_i\right) \qquad (3)$$

For compressible flows, a density-weighted, time-average decomposition (also called Favre average) is used: variables are then defined as $\widetilde{\Phi} = \overline{\rho\Phi}\big/\overline{\rho}$ and $\Phi = \widetilde{\Phi} + \Phi^{"}$.

The Reynolds tensor is given by a Boussinesq hypothesis and the two-equation k-w with SST correction [7].

2.2 Gas phase chemistry

The mass of non-ideal combustion products is very low, but the consequences for atmospheric chemistry are significant. When interacting together and with ambient species during the mixing process, emitted materials undergo chemical transformations that determine their atmospheric impact by direct or indirect effects involving secondary products. Their concentration depends on various parameters such as the engine type, the fuel composition, the plume dilution and the ambient conditions.

The main gaseous emissions from aircraft engines are carbon dioxide CO_2 and water vapor $H_2O_{(v)}$. Minor species are nitrogen oxides NO_x, carbon oxide CO and hydrocarbons, which are regulated. Furthermore, sulfur is found in aircraft fuel at different concentrations. Sulfur products are quite important because they act as aerosol precursors, which can promote homogenous nucleation and form volatile sulfate aerosols. As sulfur products are also expected to activate soot-particle surfaces and enhance contrail formation, it is highly desirable to know the amount of sulfur species in the plume.

A kinetic reaction scheme has been implemented in CEDRE based on [8] and [9]. The scheme consists of 23 species and 60 reactions, including SO_x, NO_x and HO_x chemistry. The knowledge of the behavior of species such as NO_x and HO_x, is also needed, since they play a major role in air quality and climate-change issues, especially through ozone formation. Furthermore, they are also necessary to predict SO_x concentration, since there are many interactions between NO_x, HO_x and SO_x in the plume.

2.3 Simplified microphysical model

The plume mixture is assumed to be initially made of exhaust gases and soot particles, while species are considered as ideal gases. Soot particles are assumed to be spherical for the sake of simplicity, as their fractal-like structure is too complex to account for, especially in a CFD code, and the impact of such a property remains difficult to assess.

A process of adsorption for soot coating with sulfuric acid and sulfur trioxide formed in the plume leads to soot activation (soot become hydrophilic after being hydrophobic). The used chemical kinetics scheme described above, determines the concentration of the sulfur compounds formed from the sulfur initially in the fuel. The chemical activation process is based on the work reported in [10].

The freezing process is supposed to be immersion freezing from a thin liquid layer, and we assume that turbulence does not promote ice growth in any particular direction. Gas and particles (soot and induced ice crystals) are assumed to be in dynamic and thermal equilibrium [3].

Particles are carried by the gas as a passive scalar using an Eulerian approach, the number density per cell calculated with the following transport equation:

$$\frac{\partial}{\partial t}\left(\overline{\rho}\widetilde{N}_p\right) + \frac{\partial}{\partial x_j}\left(\overline{\rho}\tilde{u}_j\widetilde{N}_p\right) = \frac{\partial}{\partial x_j}\left(\overline{\rho}D_{diff}\frac{\partial \widetilde{N}_p}{\partial x_j} - \overline{\rho}\widetilde{u_j^{"}N_p^{"}}\right) \qquad (4)$$

Figure 1 presents the evolution of the saturation over liquid water and ice against the age of the plume (time or distance behind the jet-exhaust). These curves are used to explain the principle of particle growth in the contrail. Once soot particles are activated according to an adsorption mechanism [3] with SO_3 and H_2SO_4 molecules, heterogeneous nucleation of water vapor (surrounded the soot particles) is likely to appear once saturation over liquid water is reached (see point A, Figure 1). As soot particles are activated, we assume that a thin water film forms and that liquid water freezes instantaneously.

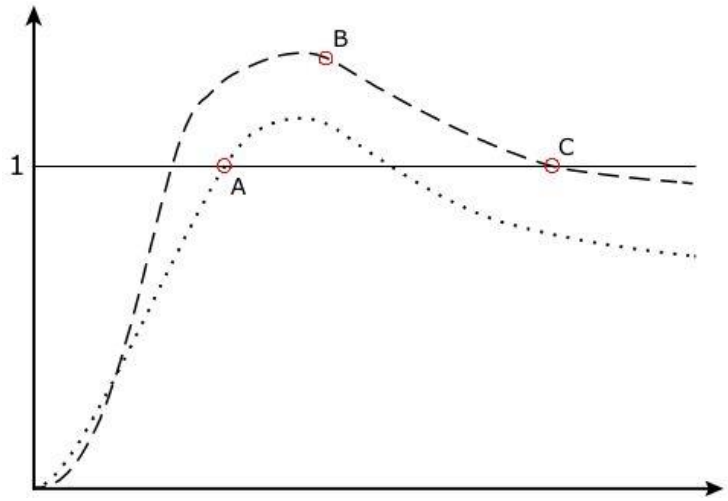

Figure 1: Illustration of the evolution of the saturation over ice (dashed curve) and over liquid water (dotted curve) in the plume function of the time (age of the plume).

While saturation over ice is above unity (supersaturation conditions, point C, Figure 1), the plume water vapor is very efficiently deposited on the ice particles. This process stops when it falls below unity.

3.0 NUMERICAL SIMULATION SETUP

In this paper, a parametric study evaluating the impact of atmospheric conditions (here temperature and relative humidity) on the properties of possibly forming contrails is presented. Three different conditions have been considered. The first one, corresponding to an ambient temperature of 223 K and a relative humidity of 41 %; the second one corresponding to the same ambient temperature but with 0 % of ambient humidity (dry air); the third one corresponds to 230 K and 19 % of relative humidity. Simulations have been carried out considering realistic aircraft geometry, presented hereunder.

3.1 Aircraft configuration

In order to study the effect of the wake's dynamics on contrail formation, a realistic aircraft configuration is needed. Such realistic geometries are usually aircraft makers proprietary and difficult to be used as a research platform. The CRM [11] designed by NASA and Boeing appears to be a good solution since it is a well-known, well documented and open source geometry. This configuration is representative of a B777 with a wingspan of about 60 m. A modified version as described in [12] [13] has been used for the study (see Figure 2). In the modified model, all elements such as wing, fuselage, nacelle, pylon, horizontal and vertical tail plane have been included. Moreover, because the original CRM has a through flow nacelle, specific internal engine geometry has been designed to allow simulation of a dual-stream jet, with a bypass ratio of 12, representative of modern aircraft engines [5].

Figure 2: Modified CRM wing/body/engine configuration, highlighting engine primary core (red) and bypass flow (orange)

3.2 Computational domain

The computational domain includes the aircraft geometry with far limits upstream of the plane and on the sides to minimize the effect of boundary limits on the flow. The extension of the domain behind the wing tip is around 19 spans (more than 1 km). In cruise conditions, it corresponds to 4.5 s and still in jet regime. **Table 1** presents the computational domain dimensions for all the simulations carried out in this study. b is the wing span length (60 m).

Table 1 Computational domain

Domain size	L_x	$[-10b; 20b]$
	L_y	$[0; 10b]$
	L_z	$[-10b; 10b]$

3.3 Grid mesh adaptation procedure

As we want to investigate contrail formation in a multiphysics approach and its subsequent evolution, we need to simulate very different processes, with various characteristic time and length. CFD is computationally very demanding and it has been necessary to optimize the mesh, so that it is refined only in the area of interests, where physics needs to be captured in detail.

To meet those requirements, a mesh adaptation technique with "feflo" [14] has been performed using a surface and volume anisotropic re-meshing based on a prescribed Riemannian metric field. The complete adaptive algorithm for steady simulations is composed of the following steps as depicted:

1. Compute the flow field (i.e. converge the flow solution on the current mesh);
2. Compute the metric-based error estimate;
3. Generate a unit mesh with respect to these metric fields;
4. Re-project the surface mesh onto the true geometry using the CAD data;
5. Interpolate the flow solution on the new adapted mesh;
6. Goto 1.

3.4 Boundary and initial conditions

Table 2 presents the atmospheric and engine-exhaust conditions used for the 3 simulations carried out to address the parametric study. According to Schmidt-Appleman criterion, the ambient conditions for the 3 simulations have been selected in order to form (case #1) or not (case #2 and #3) contrails. The case #1 is the reference case: for case #2, the relative humidity has been set to 0% while remaining temperature constant; for case #2, the temperature has been increased (+7 K) leading to a decrease of the relative humidity with respect to liquid water (19% instead of 41%).

Table 2 Atmospheric and engine-exhaust conditions

	Ambient conditions				Engine core flow			Engine Bypass flow		
#	$\overline{\mathrm{T}}$ (K)	$\tilde{u}$ (m/s)	$\overline{p}$ (Pa)	RH (%)	$\overline{T}_t$ (K)	$\overline{p}_t$ (Pa)	$\overline{N}_s$ (#/ cm^3)	$\overline{T}_t$ (K)	$\overline{p}_t$ (Pa)	$\overline{N}_s$ (#/ cm^3)
1	223.15	254.38	26437	41	626.41	53001	10^{12}	297.23	69961	0
2	223.15	254.38	26437	0	626.41	53001	10^{12}	297.23	69961	0
3	230.15	254.38	26437	19	626.41	53001	10^{12}	297.23	69961	0

Table 3 sums up the boundary conditions imposed in the computational domain. As mentioned above, the far field conditions (in front and in the sideway of the aircraft) have been rejected to 10 times the span length to ensure that it would not affect the near field. Moreover, a symmetry condition has been used to simulate the half aircraft.

Table 3 Boundary conditions

Boundary conditions	$x = -10b$	Inlet
	$x = 20b$	Outlet
	$y = 0$	Symmetry
	$y = 10b$	Outlet
	$z = -10b$	Slip (normal stress set to 0)
	$z = 10b$	Slip (normal stress set to 0)

Table 4 describes the initial conditions for gas species in the exhaust core and the ambient air, in mass fraction (kg per kg of Air). The engine-core-flow and bypass-flow properties were taken from [15] for the CFM56-3. The ambient air is given in [8].

Table 4 Initial condition for the gas species volume mixing ratio

k	**Molecular Name**	**Exhaust Core**	**Ambiant Air**
1	*O*	0.00	0.00
2	O_2	$1.49\text{x}10^{-1}$	$2.32\text{x}10^{-1}$
3	O_3	0.00	$4.97\text{x}10^{-7}$
4	*H*	0.00	0.00
5	H_2	0.00	$6.26\text{x}10^{-8}$
6	*OH*	$5.93\text{x}10^{-6}$	0.00
7	HO_2	0.00	0.00
8	H_2O	$2.20\text{x}10^{-2}$	$6.08\text{x}10^{-5}$
9	H_2O_2	0.00	0.00
10	*NO*	$6.90\text{x}10^{-5}$	0.00
11	NO_2	$1.06\text{x}10^{-5}$	0.00
12	NO_3	0.00	0.00
13	N_2O_5	0.00	0.00
14	HNO_2	0.00	0.00
15	HNO_3	0.00	0.00
16	*CO*	$2.90\text{x}10^{-5}$	$3.87\text{x}10^{-8}$
17	CO_2	$4.82\text{x}10^{-2}$	$5.01\text{x}10^{-4}$
18	*SO*	0.00	0.00
19	SO_2	$1.15\text{x}10^{-5}$	0.00
20	SO_3	0.00	0.00
21	HSO_3	0.00	0.00
22	H_2SO_4	0.00	0.00
23	*N2*	$1-\sum_{k=1}^{22} y_k$	$1-\sum_{k=1}^{22} y_k$

4.0 RESULTS

4.1 Grid mesh optimization and jet vortex interaction

In this section, the grid mesh optimization is shown to handle with the previous requirements to capture the wake and the exhaust-jet. Figure 3 to Figure 5 illustrate the cut at several span downstream of the wingtip. For each cut plane, six meshes are presented, (Figure 3 (a) to Figure 5 (a)) from left to right, in order to show the grid mesh optimization done with the code "feflo". The parameter used for the optimization is based on the norm of the cross flow velocity V_s, the main flow is supposed to be aligned with x-direction. In the present study, it reads in:

$$V_s = \sqrt{V_y^2 + V_z^2} \qquad (5)$$

The main interest of this sensor is that there is no need of derivative calculations, contrarily to vorticity for example. Furthermore, it is expected to be efficient for capturing the jet-wake interaction which may be illustrated trough temperature fields (Figure 3 (b) to Figure 5 (b)). On Table 5, the six grid mesh characteristics are summarized in order to illustrate the number of elements.

Table 5 Grid mesh characteristics with optimization

Grid mesh #	Number of tetrahedron
1	6,701,472
2	3,951,416
3	4,521,308
4	5,295,037
5	7,260,068
6	10,861,983

This technique has successfully been used in previous work [5] and is systematically used now. The gain is especially in terms of mesh optimization and aerodynamics resolution.

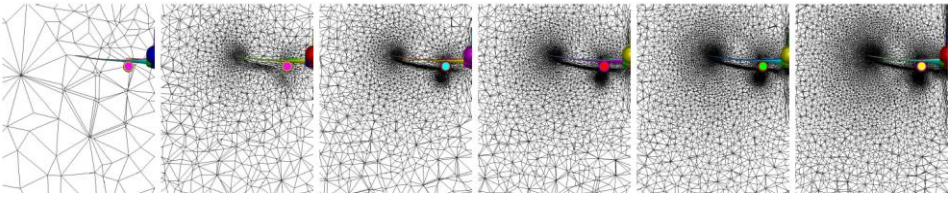

(a)

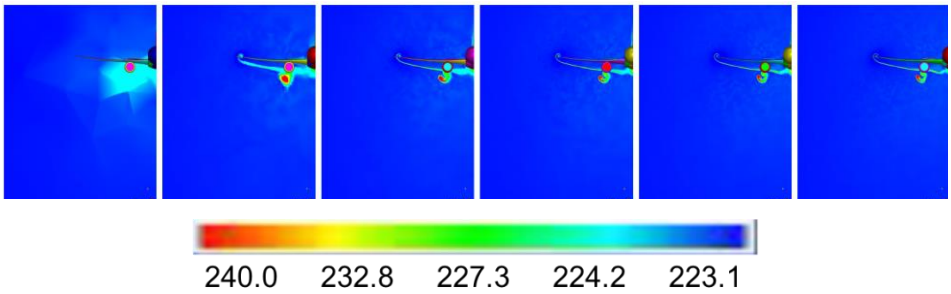

(b)

Figure 3: Cut plane at 1 span downstream of the wingtip: mesh #1 to #6 from left to right side (a) and temperature field (b)

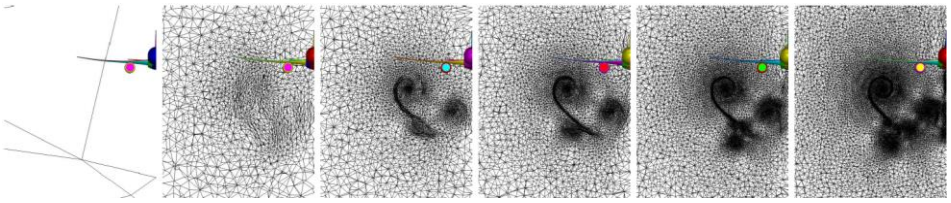

(a)

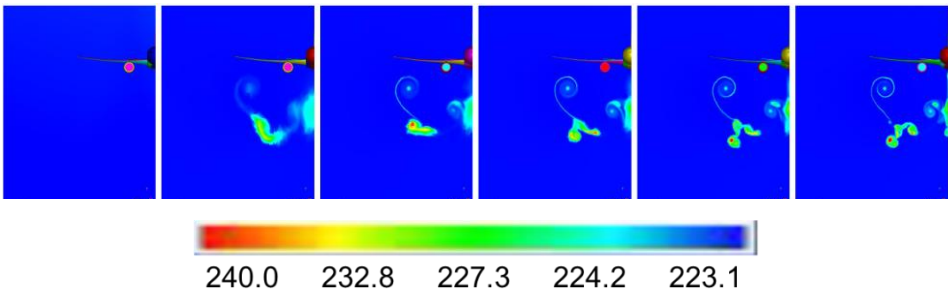

(b)

Figure 4: Cut plane at 8 span downstream of the wingtip: mesh #1 to #6 from left to right side (a) and temperature field (b)

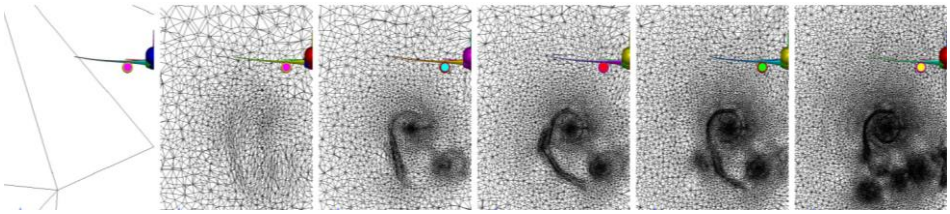

(a)

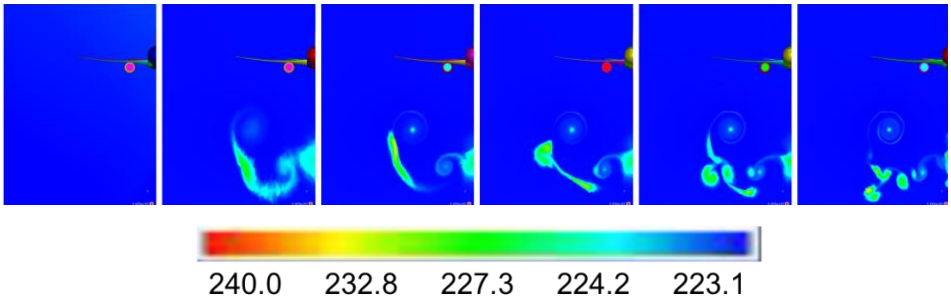

(b)

Figure 5: Cut plane at 16 span downstream of the wingtip: mesh #1 to #6 from left to right side (a) and temperature field (b)

Figure 6 give a different view of the jet vortex interaction where blue lines correspond to the vortex sheet, red lines to the core flow jet and the orange lines to the bypass flow.

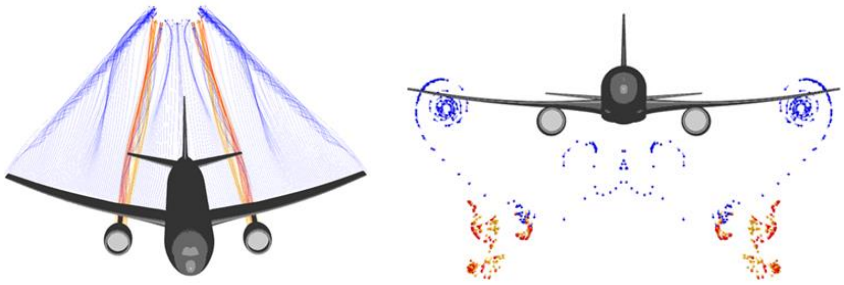

Figure 6: Evolution of the vortex sheet (blue), core flow (red) and bypass flow (orange)

The mixing process is captured with a better accuracy since simulations include both of the core flow and the bypass flow. This is crucial to estimate the plume dilution governing temperature and chemical species concentrations which pilot chemical transformation and microphysical processes responsible of contrails formation.

4.2 Gas phase chemistry

Chemical transformations are considered in simulations of contrail formation and evolution to take into account their role in soot activation. In fact, soot particulates are considered as hydrophobic at the exit of the engine. It is the interaction with gas, in particular sulfuric species, which makes them hydrophilic allowing them to play the role of condensation nuclei in the plume.

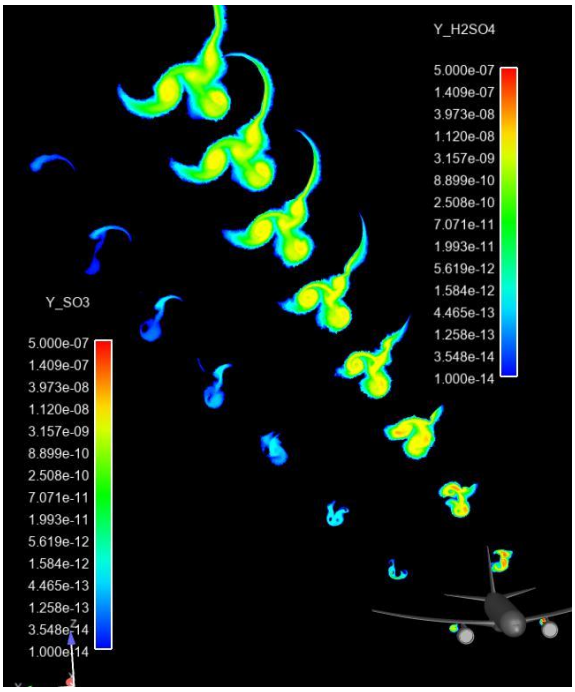

(a)

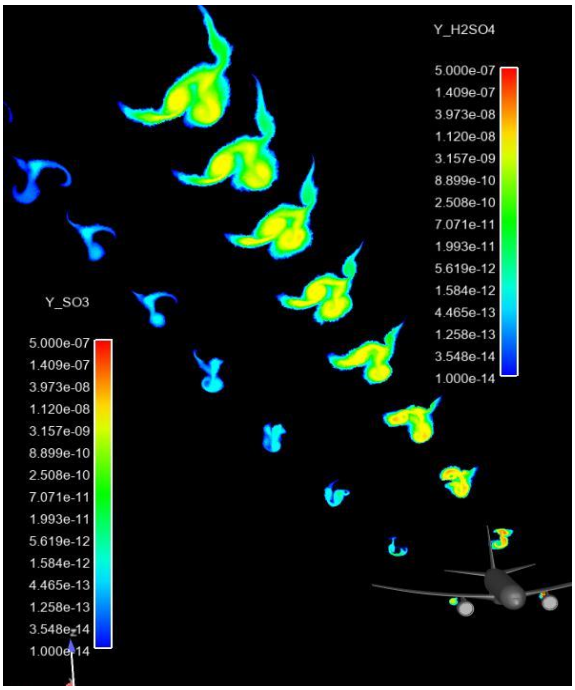

(b)

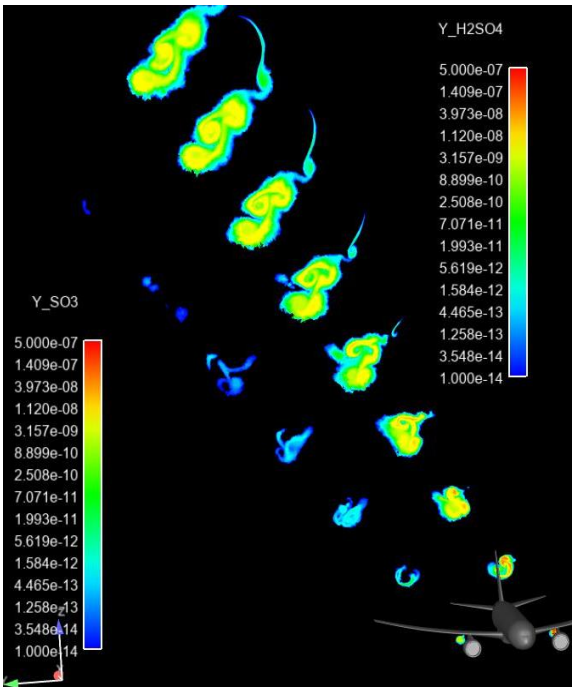

(c)

Figure 7: H_2SO_4 and SO_3 mass fraction fields downstream of the aircraft for case #1 (a), case #2 (b) and case #3 (c)

4.3 Microphysical processes and contrail formation

In addition to soot activation, ice crystals formation requires water supersaturation (saturation greater than 1) depending mainly on water concentration and temperature. First, supersaturation above liquid water is required to start water condensation on activated soot particulates. Thus, it is only in these zones (see Figure 8) that ice crystals are allowed to form.

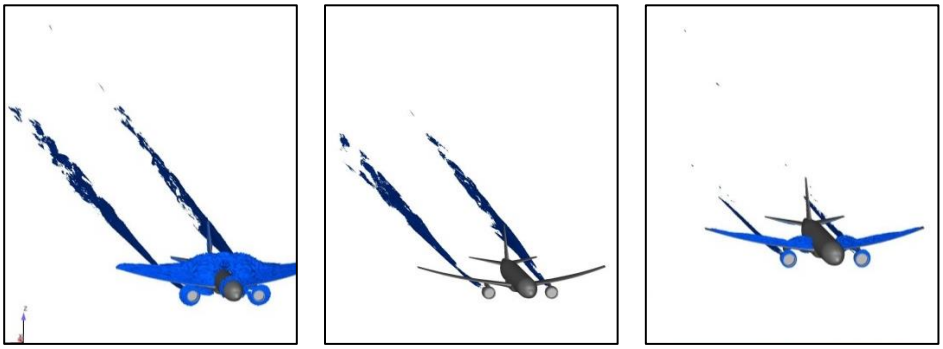

Figure 8: Supersaturation field above liquid water - from left to right, case #1, #2 and #3

The, saturation over ice then drives the evolution of ice crystals size. When saturation is greater than 1 (see Figure 9), crystals grow and when it is less than 1, crystals evaporate and their size decreases.

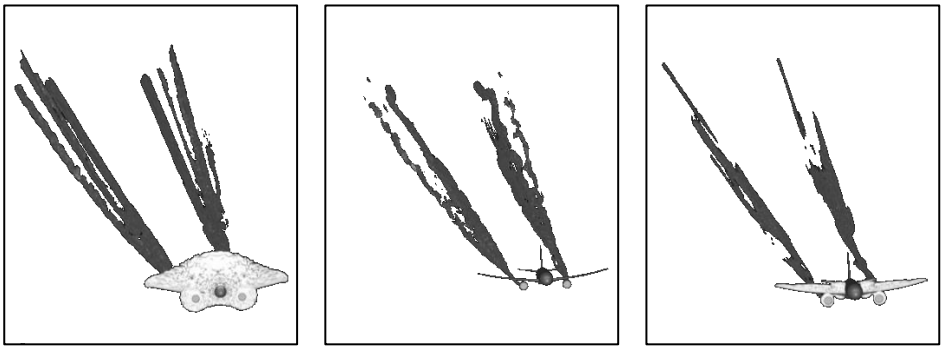

Figure 9: Supersaturation field above ice - from left to right, case #1, #2 and #3

Optical depth is a classical way to highlight the contrails visibility. The contrail is then visible if the optical depth is more than 0.01. This value depends mainly on ice crystal number and size [3]. Figure 10 (a), (b) and (c) illustrate visible contrails for the three simulated cases respectively. The results are in good agreement with the expectations. In case #2 corresponding to dry air (RH = 0 %), the contrail is thinner than in case #1. It forms due to water coming from engine exhausts but is not powered by ambient humidity comparing to case #1. In case #3, the contrail forms but disappears before reaching the end of the computational domain corresponding to one kilometer behind the aircraft. In fact, case #3 has a lower ambient relative humidity and a higher ambient temperature comparing to case #1. It leads to ice crystal evaporation making their size and number insufficient to obtain a visible contrail.

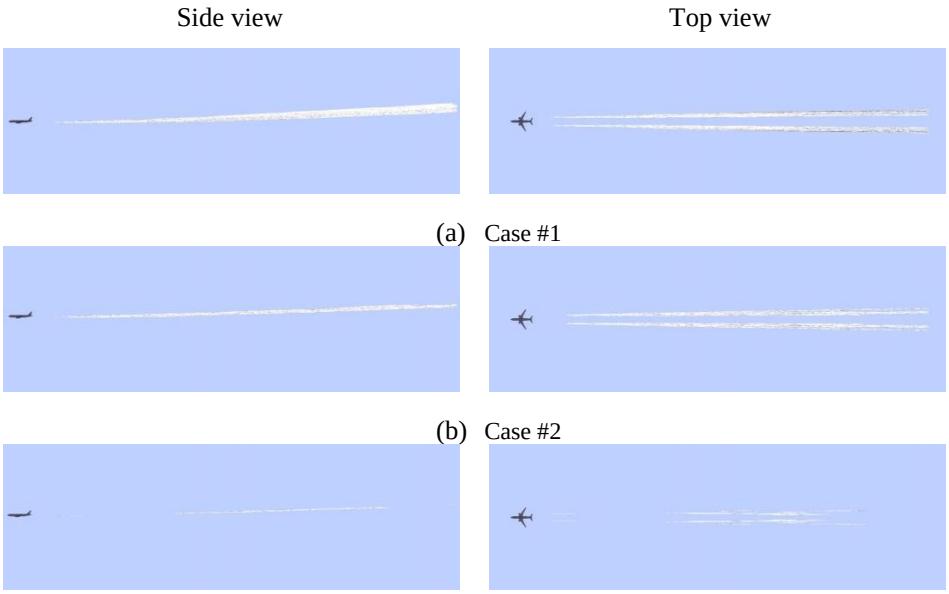

Figure 10: Contrails visualization

According to the revised Schmidt Appleman criterion [6], ambient conditions of case #1 allow contrail formation since the corresponding temperature (223 K) and relative humidity (41 %) are located above the formation threshold. In fact, point #1 in Figure 11 is located to the left of the blue dashed curve giving the temperature threshold for a relative humidity of 30 % which is valid for a humidity of 41 %. Concerning case #2 and case #3, Figure 11 shows that according to the revised Schmidt Appleman criterion, contrails don't form. Indeed, point #2 is below the green dashed curve corresponding to a relative humidity of 0 %. And point #3 is below the purple dashed curve corresponding to a relative humidity of 90 % (case #3 has a relative humidity of 19 %). However, 3D simulations predict contrail formation as shown in Figure 10 (b) and (c). Nevertheless, in case #3, the contrail evaporates quickly (Figure 10 (c)) which means that 3D simulation results and Schmidt Appleman predictions are rather in good agreement.

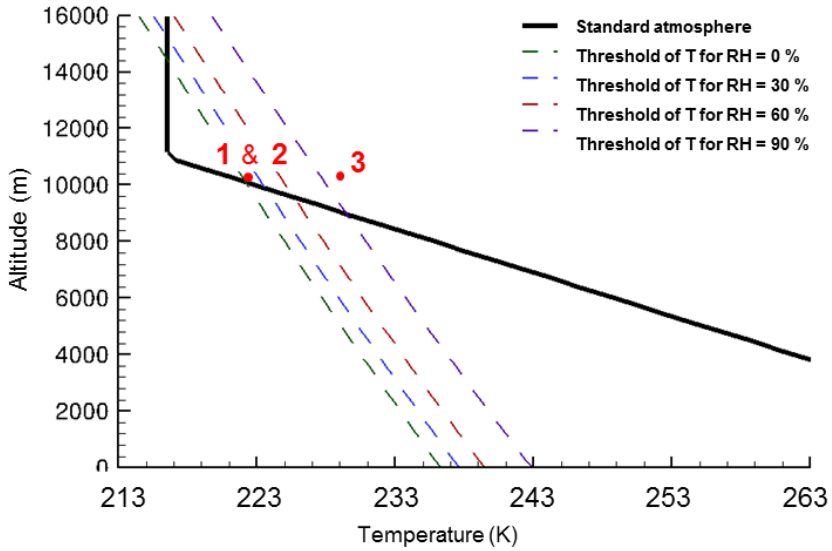

Figure 11: Temperature threshold for different values of relative humidity (dashed lines) and the location of the three cases studied #1 (RH = 41 %), #2 (RH = 0%) and #3 (RH = 19%)

In case #2, point #2 in Figure 11 is certainly above the temperature threshold but it is very close. Then even if the Schmidt Appleman criterion, calculated here from standard engine characteristics [6], predicts a non-formation of contrails, it doesn't mean that contrails don't form. In fact, there is some uncertainty concerning engine properties and the calculation method of temperature threshold doesn't take into consideration local chemical and microphysical processes in the plume. In another side, 3D simulations and the used visibility criterion cannot be considered as exact and so there remains some uncertainties in this case. However, it is interesting to note that the contrail obtained using 3D simulations is relatively thin (comparing to case #1) and it may evaporate in the few following seconds.

In fact, the objective is not to determine whether on or the other approaches is the best. It is important to keep both methods. In fact, the first one allows a rapid estimation of temperature thresholds of contrail formation. Whereas the second is necessary to analyse precisely the involved phenomena in order to estimate properly the environmental impact of contrails. It is also more appropriate for studies investigating mitigation solutions.

5.0 CONCLUSION

In the present study, three numerical simulations have been carried out in order to compare results obtained using a 3D CFD approach with the expected behavior from the Schmidt-Appleman criterion, widely used in the scientific community to identify whether or not contrail form depending on simplified thermodynamic considerations. According to this criterion, the ambient conditions have been selected in order to form or not contrails. As expected, the first case studied leads to a clear formation of contrails along the whole computational domain. In the second case, the simulation shows a contrail formed but with a thinner plume which may disappear in further. Indeed, even if Schmidt Appleman criterion doesn't predict contrail formation, the uncertainties related to both methods may explain that detailed 3D simulations give different results at least in the very near field downstream of the aircraft. Furthermore, the case studied in this paper, corresponds to ambient conditions very close to the estimated thresholds. The third case is not expected to form contrails according to Schmidt Appleman prediction whereas 3D detailed simulations give results when a small contrail form behind the aircraft but evaporate rapidly, before reaching the end of the computational domain corresponding to about one kilometer behind the aircraft. Supplementary simulations and analysis will be carried out to learn more about the improvements that should be performed in the future. Thus, the main perspectives to be explored in the future are:

- To identify the possibility of enhancing the Schmidt Appleman criterion itself, thanks to more detailed simulations including modelling of aerodynamics, chemical and microphysical processes, such as those presented here. In order to be of practical use, the way to improve the criterion should remind simple: this will be mandatory;
- To study and identify precisely how to limit or even to avoid contrail formation or at least, to control contrail properties in the near field of the aircraft where this one's characteristics can still act. The objective is for instance to lead to their evaporation before reaching a possible persistence phase only dependent on ambient atmospheric conditions.

The main goal of these studies is to participate to the efforts aiming to reduce the environmental impact of contrails and aircraft emissions in general.

ACKNOWLEDGMENTS

The authors would like to acknowledge the French Civil Aviation (DGAC) for their funding in the frame of the PHYWAKE program.

REFERENCES

[1] D. S. Lee, D. W. Fahey, P. M. Forster, P. J. Newton, R. C. N. Wit, L. L. Lim, B. Owen and R. Sausen, "Aviation and global change in the 21st century Atmospheric Environment," *Atmospheric Environment,* vol. 43, no. 22-23, pp. 3520-3537, 2009.

[2] A. Refloch, A. Courbet, A. Murrone, P. Villedieu, C. Laurent, P. Gilbank, J. Troyes, L. Tesse, G. Chaineray, J.-B. Dargaud, E. Quemerais and F. Vuillot, "Cedre Software," *Aerospace Lab,* no. 2, 2011.

[3] J.-C. Khou, W. Ghedhaïfi, X. Vancassel and F. Garnier, "Spatial simulation of contrail formation in near-field of commercial aircraft," *Journal of Aircraft,* vol. 52, pp. 1927-1938, 2015.

[4] J.-C. Khou, W. Ghedhaïfi, X. Vancassel, E. Montreuil and F. Garnier, "CFD simulation of contrail formation in the near field of a commercial aircraft: Effect of fuel sulfur content," *Meteorologische Zeitschrift,* 2017.

[5] E. Montreuil, W. Ghedaïfi, V. Chmielarski, F. Vuillot, F. Gand and A. Loseille, "Numerical simulation of contrail formation on the common research model wing/body/engine configuration," in *10th Space and Atmospheric Environment AIAA conference*, Atlanta, 2018.

[6] U. Schumann, "On conditions for contrail foirmation from aircraft exhauts," *Meteorologische Zeitschrift,* vol. 5, no. 1, pp. 4-23, 1996.

[7] F. Menter, "Two-equation eddy-viscosity turbulence models for engineering applications," *AIAA journal,* vol. 32, no. 8, pp. 1598-1605, 1994.

[8] B. Kärcher, M. Hirschberg and P. Fabian, "Smallscale chemical evolution of aircraft exhaust species at cruising," *J. Geophys. Res,* vol. 101, 1996.

[9] B. Kärcher, T. Peter, U. Biermann and U. Schumann, "The Initial Composition of Jet Condensation Trails," *J. Atsmospheric Sci.,* vol. 53, pp. 3066-3083, 1996.

[10] H. Wong, P. Yelvington, M. Timko, T. Onasch, R. Miake-Lye, J. Zhang and I. Waitz, "Microphysical Modeling of Ground-Level Aircraft-Emitted Aerosol Formation: Roles of Sulfur-Containing Species," *J. Prop. Power,* vol. 24, p. 590–602, 2008.

[11] J. Vassberg, M. DeHaan, M. Rivers and R. Wahls, "Development of a Common Research Model for Applied CFD," in *26th AIAA Applied Aerodynamics Conference*, Honolulu, 2008.

[12] D. Hue, S. Péron, L. Wiart, O. Atinaults, E. Gournay, P. Raud, C. Benoit and J. Mayeur, "Validation of a near-body and off-body grid partitioning methodology for aircraft aerodynamic performance prediction," *Computers and Fluid,* vol. 117, pp. 196-211, 2015.

[13] A. Cartieri, D. Hue, Q. Chanzy and O. Atinault, "Experimental Investigations on Common Research Model at ONERA-S1MA–Drag Prediction Workshop

Numerical Results," *Journal of Aircraft*, 2017.

[14] A. Loseille, F. Alauzet, A. Dervieux and P. Frey, "Achievement of second order mesh convergence for discontinuous flows with adapted unstructured mesh adaptation," in *AIAA conference*, 2007.

[15] F. Garnier, C. Beaudoin, P. Woods and N. Louisnard, "Engine emission alteration in the near field of an aircraft," *Atmos. Env. Geophys. Res. Lett.*, vol. 31, no. 12, pp. 1767-1781, 1997.